

# Simultaneous Quantification of the Interplay Between Molecular Turnover and Cell Mechanics by AFM–FRAP

Mark Skamrahl, Huw Colin-York, Liliana Barbieri, and Marco Fritzsche\*

**Quantifying the adaptive mechanical behavior of living cells is essential for the understanding of their inner working and function. Yet, despite the establishment of quantitative methodologies correlating independent measurements of cell mechanics and its underlying molecular kinetics, explicit evidence and knowledge of the sensitivity of the feedback mechanisms of cells controlling their adaptive mechanics behavior remains elusive. Here, a combination of atomic force microscopy and fluorescence recovery after photobleaching is introduced offering simultaneous quantification and direct correlation of molecule kinetics and mechanics in living cells. Systematic application of this optomechanical atomic force microscopy–fluorescence recovery after photobleaching platform reveals changes in the actin turnover and filament lengths of ventral actin stress fibers in response to constant mechanical force at the apical actin cortex with a dynamic range from 0.1 to 10 nN, highlighting a direct relationship of active mechanosensation and adaptation of the cellular actin cytoskeleton. Simultaneous quantification of the relationship between molecule kinetics and cell mechanics may thus open-up unprecedented insights into adaptive mechanobiological mechanisms of cells.**

Living cells are biomechanical entities. Recent research indicates that they regulate their cell mechanics not exclusively downstream of signaling events triggered by for instance ligand–receptor binding, but that they employ a diversity of feedback mechanisms to dynamically adjust their mechanics in response to extrinsic conditions.<sup>[1–5]</sup> This remarkable attribute of cells to modulate their mechanics involves biochemical processes between a range of proteins, subcellular structures, and organelles, but is primarily related to the dynamic nature

of their actin cytoskeleton.<sup>[5–9]</sup> Despite the significance for cell function,<sup>[10,11]</sup> our understanding of the interplay of cell mechanics and its underlying actin kinetics controlling the adaptive mechanical behavior of cells remains at best correlative from independent measurements.


Fluorescence recovery after photobleaching (FRAP) is perhaps the most successful quantification methodology of molecule kinetics and dynamics, owing to its versatility to measure reaction and diffusion dynamics at the right spatiotemporal scales.<sup>[12–14]</sup> In a typical FRAP experiment, a small region of interest (ROI) is bleached by a short exposure to high-power laser light, and subsequently the recovery of fluorescently tagged molecules is monitored over time.<sup>[15–18]</sup> The shape of the FRAP recovery curve, the so-called mobile fraction, reflects all of the complexity of the reaction diffusion dynamics of the molecule of interest. Using a theo-

retical model or numerical simulations for the analysis of the molecular actions combined with knowledge of the recovery time(s) of the respective molecule, the reaction kinetics and diffusion dynamics can be calculated and interpreted.<sup>[19–21]</sup> Analysis of the experiments reveals whether a molecule undergoes reaction kinetics or diffusion dynamics or a combination of both processes.<sup>[13,22]</sup> The presence of a substantial immobile fraction may be the result of the loss of fluorescence due to imaging as experienced by the fluorescent molecules during image acquisition, or it may signify that recovery has been followed over a duration that is short in comparison with the molecule's actual recovery time.<sup>[13]</sup> To this end, FRAP has been employed to identify and quantify the different types of filamentous actin (F-actin), their turnover dynamics, and lengths in the actin cortex, lamellipodium, and stress fibers.<sup>[22–26]</sup>

Atomic force microscopy (AFM) is the most broadly used quantification methodology of cell mechanics. AFM allows the precise quantification and application of mechanical forces on the apical cell surface with piconewton (pN) resolution.<sup>[27–31]</sup> For the application of mechanical force over a microscaled subregion of a cell, the cantilever tip is typically functionalized with a micron-sized fluorescent bead, and then exerted against the apical cell surface. Using AFM electronic feedback loops allows the recording of nanoscale force indentations of the cell surface as a function of the applied constant mechanical force. For example, this type of approach has been applied to investigate the biological behavior and function of living cells in response to external mechanical force.<sup>[32,33]</sup>

M. Skamrahl, Dr. H. Colin-York, L. Barbieri, Dr. M. Fritzsche  
MRC Human Immunology Unit  
Weatherall Institute of Molecular Medicine  
University of Oxford  
Headley Way, Oxford OX3 9DS, UK  
E-mail: marco.fritzsche@rdm.ox.ac.uk

Dr. M. Fritzsche  
Kennedy Institute for Rheumatology  
Roosevelt Drive  
University of Oxford  
Oxford OX3 7LF, UK

 The ORCID identification number(s) for the author(s) of this article can be found under <https://doi.org/10.1002/sml.201902202>.

© 2019 The Authors. Published by WILEY-VCH Verlag GmbH & Co. KGaA, Weinheim. This is an open access article under the terms of the Creative Commons Attribution License, which permits use, distribution and reproduction in any medium, provided the original work is properly cited.

DOI: 10.1002/sml.201902202

Hence, efforts to understand the adaptive mechanical behavior of cells separately quantified cell mechanics by AFM and molecule dynamics by FRAP, and thus inferred a relationship through correlation upon different experimental conditions, precluding knowledge of the exact nature of cell mechanosensation and its feedback. Most attempts to understand the relationship between actin and cell mechanics employed methodologies to study independently either the actin-assembly-pathways<sup>[34–36]</sup> (via classic cell-biological methods to identify a set of responsible pathways and proteins) or cellular mechanics<sup>[2,37,38]</sup> (via mechanical tools to measure mechanical properties and forces), allowing correlative predictions, for example, about the interwoven relationship of actin kinetics, respective F-actin lengths, and cellular mechanics.<sup>[38–41]</sup> However, in-depth understanding of the feedback mechanisms of the adaptive mechanical behavior of living cells profoundly necessitates simultaneous recordings and thus time-dependent correlation of actin kinetics and cell mechanics, which separate measurements do not allow due to the lack of temporally synchronized information. Such synchronous measurements also allow the quantification of the mechanical response time, the dynamic range of mechanical forces to which adaptation is possible, and mechanical propagation length-scales at which living cells can sense and respond to external mechanical force.

Here, to overcome these challenges, we developed and applied an optomechanical platform combining AFM and FRAP, which offered the quantification of the adaptive mechanical behavior of living cells by simultaneous measurements of cell mechanics and the underlying actin kinetics. We found that cervical HeLa cells dynamically adjusted up to twofold the stress fiber F-actin turnover rates and nanoscale filament lengths within a dynamic range of 0.1 to 10 nN in response to constant mechanical force at the apical actin cortex applied through contact with a radius  $r = 5 \mu\text{m}$  bead connected to the AFM cantilever. Strikingly, the apical mechanical stress was detected by the cells at their ventral interface resulting in adaptation of the nanoscale organization of F-actin stress fibers qualitatively comparable to those in the actin cortex, highlighting a mechanical propagation length-scale equivalent of the entire cell volume. Consequently, such simultaneous experiments may thus become the methodology of choice to reveal the mechanobiological mechanisms underlying mechanoadaptation.

To quantify the effects of mechanoadaptation of the actin cytoskeleton in living cells, we combined simultaneous AFM and FRAP experiments (**Figure 1a**). This optomechanical AFM–FRAP platform consisted of JPK AFM, Leica DMI8, and Rapp OptoElectronic FRAP modules (Experimental section). The AFM module allowed the application of constant mechanical force by contact with a bead-functionalized AFM cantilever at the apical surface and proximity of the central cell plane away from the cell nucleus. Simultaneously, the FRAP module enabled measurements of the turnover dynamics of cellular structures directly underneath the cell surface-bead contact or any location within the cell volume.

To calibrate the AFM–FRAP experiments, we first optimized the FRAP protocol. To this end, we determined the diffraction-limited point spread function (PSF) of the FRAP laser (**Figure 1b**) and measured the volume of a FRAP photobleaching event in a region of interest (ROI) at two different

axial locations within a 15–20  $\mu\text{m}$  thick EGFP-functionalized polyacrylamide gel. We achieved laterally the best well-defined reduction in fluorescence of a 2  $\mu\text{m}$  diameter-sized ROI with 50% laser power when adjusting between 25% and 100% total laser power at both the glass–hydrogel interface and 4  $\mu\text{m}$  deep into the fluorescent gel (**Figure 1c**), representing the ventral and central plane of HeLa cells, respectively.

To ensure that the laser settings of the FRAP photobleaching event were compatible with and not harmful to F-actin structures in cells, we next performed FRAP experiments on ventral actin stress fibers in fixed HeLa cells fluorescently labeled with the photostable dye phalloidin-Alexa488, which was kept present in the imaging medium of the fixed cells and thus allowed phalloidin turnover measurements. Notably, extended laser power of the photobleaching event could yield permanent damage to the F-actin architecture in addition to photobleaching the fluorescent dye. Consistent with our EGFP hydrogel calibration, we achieved a well-defined 2  $\mu\text{m}$  sized ROI, sufficient fluorescence reduction, and mobile fluorescence recovery. The recovery appeared continuous throughout the ROI volume with no indication of directed fluorescence growth from the geometric sides of the actin stress fibers as it could be expected from damaged and regrowing actin stress fibers (**Figure 1d**). Note, the FRAP calibration experiments were terminated after 600 s in the fixed cells because of sample drift, and partial 80% fluorescence mobile recovery of phalloidin was sufficient for the evaluation of the direction of fluorescence increase considering 10% loss of fluorescence due to photobleaching and immobile fraction.

Having optimized the FRAP protocol, we next established an experimental protocol for a full typical AFM–FRAP experiment (**Figure 1e–g**). We approached the cell with the bead-cantilever until initial contact (**Figure 1e**), then indented the cell surface by gradually further decreasing the distance and increasing the force until the maximal predefined force was reached, which was then maintained constant over the time of the AFM–FRAP experiment. Once constant force was established, we waited for 2 min post initial contact to equilibrate the bead-cantilever cell surface interaction, and subsequently executed the previous FRAP protocol simultaneously to the force application by AFM (**Figure 1f**), allowing turnover measurements under constant mechanical force. Finally, the cantilever would be retracted once full FRAP recovery was completed and the AFM–FRAP protocol was repeated in a different HeLa cell for statistical robustness (**Figure 1g**).

To gain a quantitative understanding of the length-scale and sensitivity of mechanoadaptation in living cells, we first set out to characterize the actin cytoskeleton in control conditions in the absence of mechanical force. Because we reasoned to perform the AFM–FRAP experiment at a ROI representative for the global mechanical stiffness, we acquired a stiffness spectroscopy map of a HeLa cell applying the cantilever functionalized with a radius  $r = 5 \mu\text{m}$  bead (**Figure 2a,b**). We primarily aimed at quantifying the turnover dynamics in actin stress fibers and cortex without any contributions from the cytoplasmic actin network or cellular organelles such as the nucleus while applying a global mechanical stimulus. Hence, spectroscopic evaluation suggested a representative ROI location at the extended HeLa cell body away from the cell nucleus

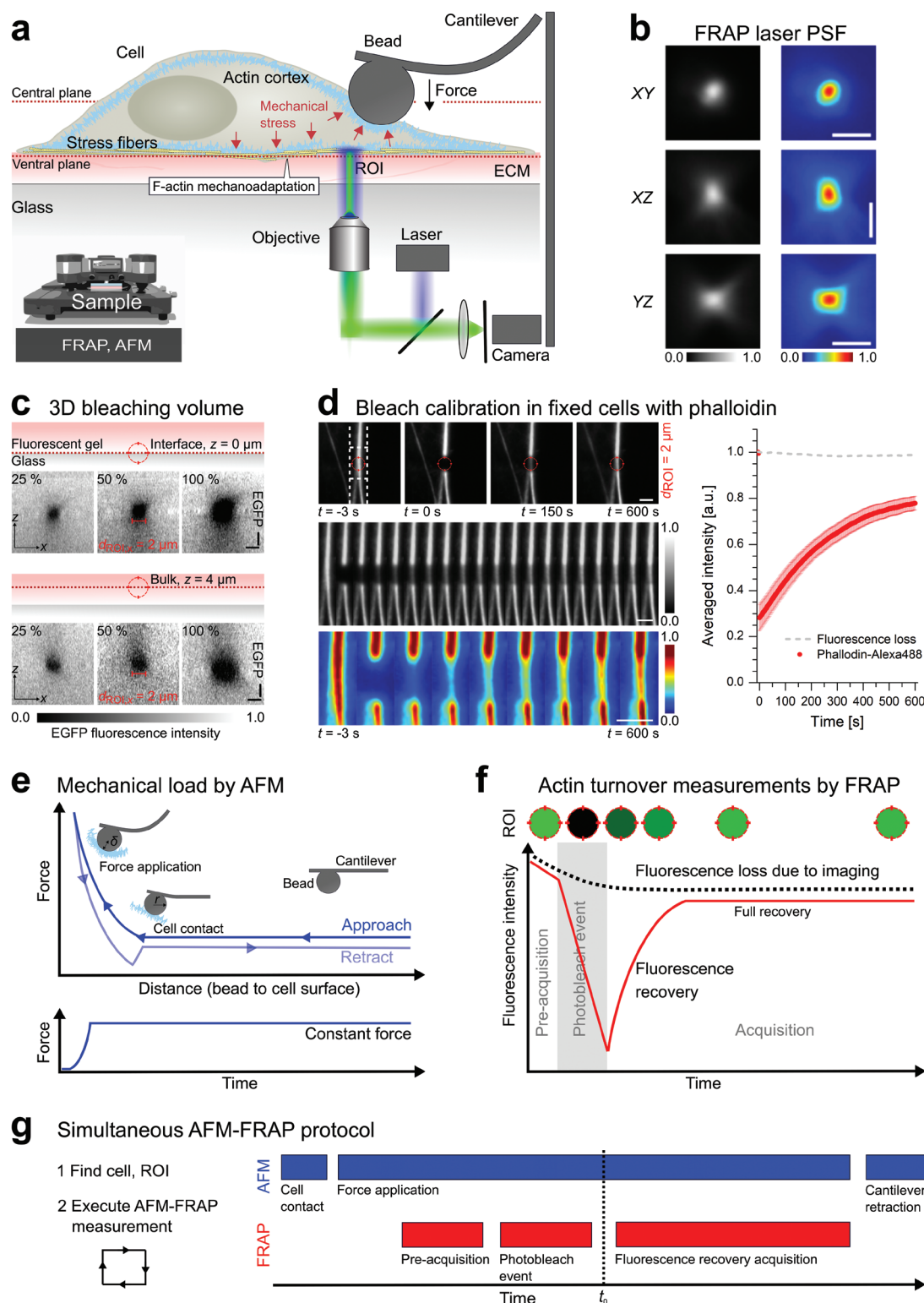


**Figure 1.** Establishment and calibration of the optomechanical AFM–FRAP platform. a) Schematic of the AFM–FRAP setup illustrating the experimental power of simultaneous quantification of molecule kinetics and cell mechanics. b) Representative images of the diffraction-limited FRAP PSF in XY, XZ, and YZ orientation. Scale bars are 2  $\mu\text{m}$  (XY) and 4  $\mu\text{m}$  (XZ and YZ). c) Calibration of the FRAP ROI at both the glass–hydrogel interface and 4  $\mu\text{m}$  deep into the hydrogel for different laser powers. Scale bars are 2  $\mu\text{m}$  (in x-direction) and 4  $\mu\text{m}$  (in y-direction). d) Evaluation of FRAP photobleaching events on ventral actin stress fibers in fixed HeLa cells fluorescently labeled with phalloidin-Alexa488. Kymographs illustrate fluorescence recovery in the ROI (red). Scale bars: 2  $\mu\text{m}$ . e,f) AFM and FRAP protocols for the application of mechanical force and measurements of the turnover kinetics in living HeLa cells. g) Workflow of a typical AFM–FRAP experiment.



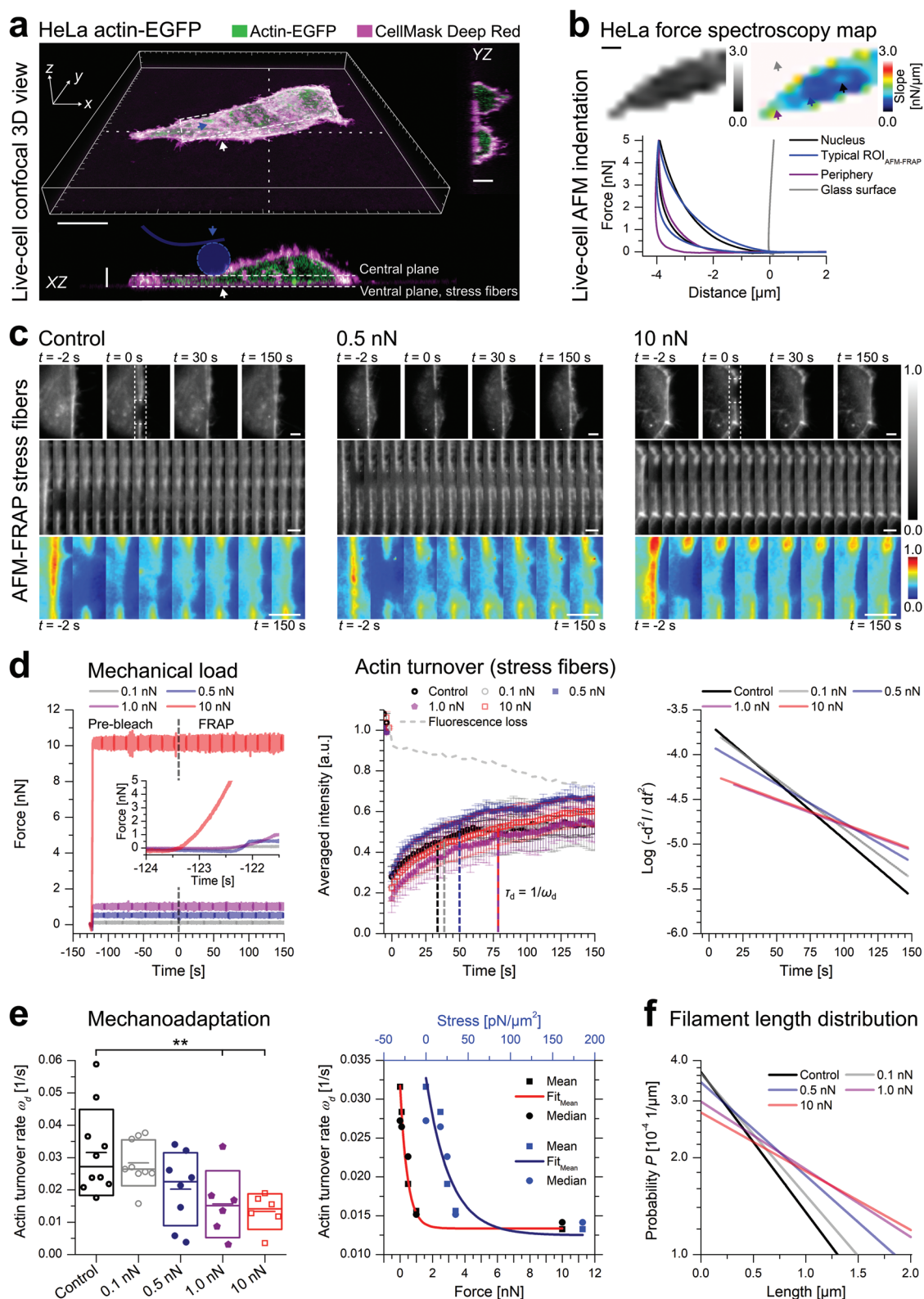


**Figure 2.** Application of AFM-FRAP experiments in ventral actin stress fibers. a) Representative experimental AFM-FRAP live-cell setup showing the application of mechanical force to the central plane at the apical surface of a HeLa cells with a bead-functionalized cantilever (indicated in blue, blue arrow). Simultaneous FRAP experiments were acquired in ventral actin stress fibers (white arrow head). Scale bars are 10  $\mu\text{m}$  ( $x/y$ -plane) and 4  $\mu\text{m}$  ( $z$ -plane in horizontal views). b) Spectroscopic validation of the stiffness distribution and corresponding force-distance curves for a typical HeLa cell. Scale bar is 10  $\mu\text{m}$ . c,d) AFM-FRAP experiments illustrated in kymographs, force-time plots, and FRAP recovery curves, and their corresponding

**Table 1.** Summary of FRAP fitting parameters in living HeLa cells. Single-component fitting of FRAP recovery curves revealed the turnover kinetics of the ventral actin stress fibers (mean  $\pm$  SD). Fitting parameters of the turnover rates and respective abundance for formin-mediated F-actins in stress fibers are given by  $\omega_{\text{stress fibers, formin}}$  and  $f_{\text{stress fibers, formin}}$ . Two stars (\*\*) indicate a significance level of  $p < 0.01$ .

Condition	Control	0.1 nN	0.5 nN	1.0 nN	10 nN
$\omega_{\text{stress fibers, formin}}$ [1/s]	$0.032 \pm 0.013$	$0.028 \pm 0.007$	$0.020 \pm 0.011$	$0.016 \pm 0.010$	$0.013 \pm 0.005$
$f_{\text{stress fibers, formin}}$	$1.0 \pm 0.1$	$1.0 \pm 0.1$	$1.0 \pm 0.1$	$1.0 \pm 0.1$	$1.0 \pm 0.1$
$p$ (compared to control)	–	$p = 0.84$	$p = 0.17$	$p < 0.01^{**}$	$p < 0.01^{**}$

(Figure 2b). We also avoided the cell edge to mitigate effects of the underlying stiffer glass and to probe a mechanically representative area, resulting in an optimal position in between the nucleus and the cell boundary (Figure 2b).

Applying FRAP at the central actin cortex in live HeLa cells expressing fluorescently labeled actin-EGFP, we found two processes contributing to fluorescence recovery. Analysis of the FRAP experiments revealed an average turnover rate of  $\omega_{\text{cortex, Arp2/3, Ctrl}} = 0.55 \pm 0.12$  (mean  $\pm$  SD) 1/s for the Arp2/3-mediated F-actin and  $\omega_{\text{cortex, formin, Ctrl}} = 0.040 \pm 0.009$  (mean  $\pm$  SD) 1/s for the formin-mediated F-actin in control conditions consistent with our previous measurements (see Experimental section),<sup>[22,23]</sup> which were dominating fluorescence recovery on short time-scales and long time-scales, respectively. In contrast to cortical F-actin, actin stress fibers have been shown to be constituted by primarily formin-mediated F-actin. Consistent with this expectation, our FRAP experiments on ventral stress fibers displayed only one turnover process contributing to fluorescence recovery. Analysis of the FRAP experiments yielded one turnover rate  $\omega_{\text{stress fibers, formin, Ctrl}} = 0.032 \pm 0.013$  (mean  $\pm$  SD) 1/s statistically comparable to cortical formin-mediated turnover ( $p = 0.22$  compared to second turnover kinetics in actin cortex), as reported by a full fluorescence recovery shown in kymographs, FRAP curves, and respective LogPlot functions (Figure 2c,d). Note, the LogPlot functions are logarithmic second-order derivatives of the fluorescence recovery visualizing the number of turnover processes and relative abundance as described in ref. [13]. The turnover dynamics for the corresponding cortical and stress fiber F-actins were identified previously in these HeLa cells.<sup>[22]</sup>

Having determined the turnover kinetics in live HeLa cells under control conditions, we next quantified these processes under mechanical force. Executing the full AFM–FRAP protocol at the ventral stress fibers in live HeLa cells in the presence of 1 nN constant mechanical force applied by the bead-cantilever at the central actin cortex revealed a statistically significant twofold change in the kinetics of the turnover rates of the F-actin structures from  $\omega_{\text{stress fibers, formin, Ctrl}} = 0.032 \pm 0.013$  (mean  $\pm$  SD) 1/s to  $\omega_{\text{stress fibers, formin, 1 nN}} = 0.016 \pm 0.010$  (mean  $\pm$  SD) 1/s ( $p < 0.01$ , Table 1 and Figure 2c,d), suggesting modulation of ventral actin

turnover in stress fibers in response to apical mechanical force at the actin cortex.

To explore the sensitivity of such mechano-adaptation, we systematically measured the changes in the turnover kinetics in response to mechanical force ranging between 0.1 and 10 nN. Strikingly, we found that the mean and median turnover kinetics exponentially scaled as a function of the externally applied mechanical force and stress (Figure 2e) with the strongest response at the mean character-

istic value of the exponential function at 1 nN and 35 pN  $\mu\text{m}^{-2}$  (Figure 2e and Table 1), respectively, which corresponded to an apical indentation depth of 2  $\mu\text{m}$  deflecting the cortical actin. Consistent with the exponential dependence, nonstatistically different adjustments of turnover kinetics were detected at 0.1 nN ( $\omega_{\text{stress fibers, formin, 0.1 nN}} = 0.028 \pm 0.007$  (mean  $\pm$  SD) 1/s,  $p = 0.84$ ) and 0.5 nN ( $\omega_{\text{stress fibers, formin, 0.5 nN}} = 0.020 \pm 0.011$  (mean  $\pm$  SD) 1/s,  $p = 0.17$ ) but significant differences were found at 1 nN and 10 nN with  $\omega_{\text{stress fibers, formin, 1 nN}} = 0.016 \pm 0.010$  (mean  $\pm$  SD) 1/s,  $p < 0.01$ , which corresponded to a 0.4  $\mu\text{m}$  (0.1 nN), a 1.4  $\mu\text{m}$  (0.5 nN), and 2.0  $\mu\text{m}$  (1 nN) indentation of apical cortical F-actin (Figure 2a,b). Together, the simultaneous AFM–FRAP revealed direct modulation of the F-actin kinetics in ventral stress fibers in response to apical mechanical force.

Finally, we computed the filament length distributions and their mean filament lengths of the formin-mediated F-actin in the stress fibers from the FRAP quantification (see Experimental section). We found statistically significant differences with the nanoscale architecture adjusting a maximum of twofold  $\langle L \rangle_{\text{stress fibers, formin, 1 nN}} = 2.1 \pm 0.9$  (mean  $\pm$  SD)  $\mu\text{m}$  compared to control conditions  $\langle L \rangle_{\text{stress fibers, formin, Ctrl}} = 1.0 \pm 0.45$  (mean  $\pm$  SD)  $\mu\text{m}$  ( $p < 0.01$ , Table 2 and Figure 2f). For lower external forces, we found no or minor changes in the filament lengths of F-actins of  $\langle L \rangle_{\text{stress fibers, formin, 0.1 nN}} = 1.15 \pm 0.5$  (mean  $\pm$  SD)  $\mu\text{m}$ ,  $\langle L \rangle_{\text{stress fibers, formin, 0.5 nN}} = 1.5 \pm 0.75$  (mean  $\pm$  SD)  $\mu\text{m}$  compared to control conditions ( $p = 0.84$  for 0.1 nN and  $p = 0.17$  for 0.5 nN). No further statistical differences in the F-actin filament lengths were observed in response to 10 nN of external force  $\langle L \rangle_{\text{stress fibers, formin, 10 nN}} = 2.4 \pm 1.2$  (mean  $\pm$  SD)  $\mu\text{m}$  compared to 1 nN ( $p = 0.94$ , Table 2). These measurements highlighted nanoscale F-actin length remodeling of ventral stress fibers in direct response to apical mechanical stress.

We introduced an optomechanical platform combining AFM and FRAP experiments offering simultaneous quantification and direct correlation of molecular kinetics and mechanics in living cells. We chose to quantify the effects of mechano-adaptation and their dynamic range by measuring the changes in the nanoscale turnover kinetics and filament lengths of F-actins under constant mechanical force in the ideal model system of ventral stress fibers, because they were predicted

logarithmic acceleration plots showing the mechanoadaptation of ventral actin stress fibers in control conditions and in response to external mechanical force ranging from 0.1 to 10 nN. Scale bars are 2  $\mu\text{m}$ . Corresponding mean and median turnover rates are presented in Table 1. e) Boxplot displaying the quantification of actin turnover kinetics in ventral actin stress fibers in control conditions and in response to external mechanical force ranging from 0.1 to 10 nN and turnover rate as a function of force and corresponding mechanical stress. Error bars show medians and SDs while means are indicated by a horizontal line inside the boxes. f) Quantification of the filament length distribution in control conditions and in response to external mechanical force ranging from 0.1 to 10 nN. Corresponding mean filament lengths are presented in Table 2. Two stars indicate a significance of  $p < 0.01$ .

**Table 2.** Summary of the filament lengths of ventral actin stress fibers in living HeLa cells. Computation of the mean filament length  $\langle L \rangle$  ( $\pm$  SD) of formin-mediated F-actin in ventral actin stress fibers.

Condition	Control	0.1 nN	0.5 nN	1.0 nN	10 nN
$\langle L \rangle$ [ $\mu$ m]	1.0 $\pm$ 0.45	1.15 $\pm$ 0.5	1.5 $\pm$ 0.75	2.1 $\pm$ 0.9	2.4 $\pm$ 1.2

and experimentally proven to function as mechanotransducers.<sup>[8,42,43]</sup> To this end, mechanoadaptation of the previously identified formin-mediated F-actins constituting stress fibers as well as Arp2/3- and formin-mediated F-actins in the cortical network were characterized.<sup>[22,23]</sup>

Together, our experimental and computational AFM–FRAP results paint the following picture of cytoskeletal mechanoadaptation. For actin filaments in ventral stress fibers, we strikingly measured a maximum of twofold change in the mean and median turnover kinetics and filament lengths at constant 1 nN force and 35 pN  $\mu$ m<sup>−2</sup> apical stress application, which corresponded to an indentation depth of 2  $\mu$ m of the actin cortex. Interestingly, minor modulation of the turnover kinetics was detected in response to shallow indentation depths comparable to the thickness of the actin cortex. Similarly, F-actin turnover and lengths displayed effectively no further adjustment to critically high indentation of apical cortical F-actin comparable to over half of the height of a HeLa cell.

On the basis of our work, we conclude that the simultaneous measurements and direct correlation of cell mechanics and its underlying actin kinetics is superior to independent quantification, because of the feedback mechanisms of the adaptive mechanical behavior of living cells and the additional accessible parameters such as mechanical response time, the mechanical propagation length-scale, and the ability to determine the dynamic range of mechanoadaptation. We empirically found that the dynamic range of mechanoadaptation of the actin cytoskeleton in HeLa cells is most effective at a length-scale of 2  $\mu$ m indentation allowing modulation of turnover kinetics and filament lengths on the length-scale of the complete cytoplasm possibly throughout all mechanically interlinked actin structures as a function of the externally applied stress as predicted by refs. [44,45].

One might speculate that the dynamic range of mechanoadaptation is most effective at a length-scale of a formin-mediated actin filament, which corresponded to  $\approx$ 2.0  $\mu$ m equivalent to the indentation depth at 1 nN, because formin-mediated F-actins are ten times longer than Arp2/3-mediated F-actins and known to primarily determine cellular mechanical properties such as the elastic modulus and bending rigidity of the actin cytoskeleton.<sup>[23,46]</sup> Consequently, it is feasible to speculate that the typical length-scale of a formin-mediated F-actin is critical for the sensitivity of mechanoadaptation. Consistent with this line of thought, high mechanical stress and large indentations on the length-scale of the cell height resulted in poor mechanoadaptation, which is in contrast to favored cell adhesion on hard surfaces in the gigapascal range.<sup>[6]</sup> Similarly, indentations in the order of the cortex thickness,<sup>[47,48]</sup> but small compared to the average length of formin-mediated F-actin, yielded no significant mechanoadaptation. From the mechanical point of view, formins are well known to contribute to mechanosensation.<sup>[49–51]</sup> To this end, the mechanical setting at

the apical actin cortex in our experiments could translate into pulling or pushing forces on single formin molecules in cortical F-actin and the mechanically linked stress fibers, which have been demonstrated in vitro to accelerate or de-accelerate formin's polymerization activities.<sup>[52]</sup> In contrast to such passive mechanosensation by biophysical principles, active signaling-associated mechanosensation by dedicated molecules could be responsible for the actin mechanoadaptation. In light of this argument, we waited for 2 min post force application and prior execution of the FRAP experimentation for equilibration of the external forces applied to the living cells, allowing unaccounted time for signaling responses controlling actin and associated crosslinker turnover. In addition, stress propagation and transduction by mechanical tension release through the actin cytoskeleton could also contribute to the observed mechanosensation processes.<sup>[52]</sup>

One intriguing prediction of mechanosensation is hence that tuning the activity of actin kinetics to alter filament lengths may thus be a mechanism allowing cells to adjust their dynamic range and sensitivity of mechanoadaptation. The AFM–FRAP platform offers three major types of investigations, which are not possible in independent FRAP or AFM experiments: 1) Quantitative measurements of the dynamic range of cellular mechanosensation. 2) Mechanistic study of the origin of cell mechanics: mechanical properties and mechanical force production by living cells can be dynamically interrogated in response to pharmacological and genetic treatments. 3) Mechanistic investigation of the implications of protein kinetics for cell mechanics: dissecting the molecular protein dynamics underlying cell mechanics by dynamically exerting mechanical load onto living cells. Consequently, AFM–FRAP will lay a foundation to address a plethora of open biological problems. Important examples include but are not restricted to T-cell activation, cancer cell mechanics, stem cell differentiation, cellular migration, and tissue functions. These time-dependent mechanoadaptive processes have thus far only been studied without the spatiotemporal synchronization as offered by AFM–FRAP. Simultaneous quantification of the relationship between molecule kinetics and cell mechanics may thus open up unprecedented insights into adaptive mechanobiological mechanisms of cells.

## Experimental Section

**Cell Culture:** Cell culture was performed as described in ref. [24]. HeLa cells (product 93021013, Sigma Aldrich, UK; mycoplasma tested) were cultured in sterile DMEM (Sigma Aldrich) supplemented with 10% FCS (Sigma Aldrich),  $2 \times 10^{-3}$  M L-Glutamine (Sigma Aldrich) and 1% penicillin–streptomycin–neomycin solution (Sigma Aldrich). Cells were maintained at 37 °C and 5% CO<sub>2</sub> during culturing, and handling was performed in HEPA-filtered microbiological safety cabinets. Cells were passaged every 48 h, kept subconfluent, and seeded to adhere overnight prior to experimentation.

**Generation of Stable Cell Lines:** HeLa lines stably expressing actin-EGFP were generated using a lentiviral transduction strategy. HEK-293T cells were plated in six-well plates at  $3 \times 10^5$  cells mL<sup>−1</sup>, 2 mL per well in DMEM (Sigma Aldrich) supplemented with 10% FCS. Cells were incubated at 37 °C and 5% CO<sub>2</sub> for 24 h before transfection with 0.5 mg per well each of the lentiviral packaging vectors p8.91 and pMD.G and the relevant pHR-SIN lentiviral expression vector using Genejuice



(Merck Millipore, UK) as per the manufacturer's instructions. 48 h after transfection, the cell supernatant was harvested and filtered using a 0.45 mm Millex-GP syringe (Merck Millipore) filter unit to remove detached HEK-293T cells. In all wells, 3 mL of this virus-containing medium was added to  $1.5 \times 10^6$  HeLa cells in 3 mL supplemented DMEM medium. After 48 h, cells were moved into 10 mL supplemented DMEM and passaged as described above.

**Cell Fixation and Staining:** Cell fixation was effected as described in ref. [54]. HeLa cells were washed and immersed in cytoskeleton buffer [ $50 \times 10^{-3}$  M imidazole,  $50 \times 10^{-3}$  M KCl,  $0.5 \times 10^{-3}$  M  $MgCl_2$ ,  $0.1 \times 10^{-3}$  M EDTA, and  $1 \times 10^{-3}$  M EGTA (pH 6.8)]. Petri dishes (FluoroDish, FD35-100; World Precision Instruments, UK) with adherent subconfluent HeLa cells were washed three times with 1 mL of cytoskeleton buffer. The cytoskeleton buffer was replaced with 1 mL of cytoskeleton buffer containing 0.25% glutaraldehyde and 0.5% Triton X-100, with care taken not to disturb the cells attached to the glass. Samples were fixed for 5 min at room temperature before they were washed twice with 1 mL of cytoskeleton buffer and covered with 1 mL cytoskeleton buffer containing 1:100 phalloidin-AlexaFluor488 (Life Technologies, UK). Before our FRAP calibration experiments, 20  $\mu$ L of dye-containing buffer was removed and replaced by additional 20  $\mu$ L of undiluted phalloidin-AlexaFluor488 in order to ensure sufficient amounts of the fluorophore in the medium.

**AFM–FRAP Experiments:** The optomechanical AFM–FRAP platform allowed the simultaneous execution of AFM and FRAP experiments in living cells. FRAP was effected as described in refs. [13,22] at 37 °C using a 1.4 NA 100 $\times$  oil immersion objective on a widefield fluorescence microscope (Leica DMI8, Leica Microsystems) and FRAP UGA-42-Firefly laser unit (Rapp OptoElectronic). In the FRAP experiments, a small circular ROI (diameter  $d = 2$   $\mu$ m) was centered on the basal stress fibers. The photobleaching event was executed by a single photobleaching spot of a 488 nm beam operating at 50% power of the 200 mW laser using a 1% transmission neutral-density filter to reduce the applied power finally to 0.5%. In our protocol, bleaching was realized with a single laser pulse of 2 s. The recovery of fluorescence was monitored at 10% fluorescence lamp intensity over 200 frames at 0.8 to 2 s (live cells) or 3 s (fixed cells) intervals to minimize the loss of fluorescence due to imaging. For each recovery, two time-lapse image streams were recorded before the initial bleaching, which facilitated normalization of the fluorescence signal. To assess the loss in fluorescence during observation of the recovery (due to imaging), The simultaneously recorded fluorescence signal from a nonbleached region was selected. In all cases, the rate of fluorescence loss due to the imaging was significantly smaller than the rates of fluorescence recovery, with a characteristic time of  $\approx 1000$  s, which was one order of magnitude larger than the slowest recovery time-scale observed for actin. Hence, imaging-induced fluorescence loss did not significantly affect the turnover measurements.

AFM nanoindentation tests were performed with a JPK NanoWizard IV (JPK Instruments, Germany) interfaced with the Leica DMI8. For our measurements, tipless cantilevers were used with a nominal spring constant of 0.03 N m $^{-1}$  (Arrow TL2, NanoWorld, Switzerland) functionalized with a polystyrene bead with 5  $\mu$ m radius. Contact radii and respective mechanical stress were inferred following the Hertzian theory by numerically solving  $\delta = 0.5a \ln((r + a)/(r - a))$  with the indentation depth  $\delta$ , the bead radius  $r$ , and the contact radius  $a$  for spherical indenters using MATLAB (Mathworks, USA).

**AFM Analysis:** Analysis of AFM force curves was performed using the JPK SPM Data Processing software and adapting the publicly available (GitHub) python script jpkfile. Actual spring constants of the cantilevers were determined using the thermal noise method implemented in the AFM software (JPK SPM). Before indentation tests, the sensitivity of the cantilever was set by measuring the slope of force–distance curves acquired on glass regions of the petri dish. Note, the force spectroscopy map analyzed within the 1 nN dynamic range refers to linear fitting of 10% indentation depth from 1 nN force toward the contact point.

**FRAP Analysis:** FRAP data analysis was effected as described by Fritzsche et al. in refs. [13,22]. The total fluorescence intensity in stress fibers resulted from actin monomers bound to the actin architectures

and monomers freely diffusing within these structures. Fluorescence recovery had thus contributions from i) diffusive actin and ii) from association/dissociation of actin monomers to the structures. Given the fast cytoplasmic actin diffusion coefficient ( $D \approx 15 \mu m^2 s^{-1}$  of actin in our experimental geometry), diffusion of monomers took place with a characteristic time-scale of  $\tau_{diffusion} \approx r^2/4D < 1$  s (with  $r = 1 \mu m$  being the radius of the bleached zone), which was several-fold shorter than the characteristic times of the reactions examined in this study ( $\tau \geq 10$  s). Hence, given the acquisition rate used in this study (1 to 2 s per frame), diffusive recovery was completed by the time we acquired the first post-bleach frame. Consequently, we could assume the fluorescence recovery to be solely reactive. To determine how many first-order molecular processes contributed to turnover, we fitted recovery  $I(t)$  with a combination of exponential functions  $I_i$  of the form  $I_i(t) \sim [1 - \exp(-t/\tau_{d,i})]f_i F_0$ , where  $F_0$  is the initial fluorescence of the bleached region and  $i$  is the molecular process participating to recovery. Each function  $I_i(t)$  represents the contribution of the molecular process  $i$  to the total recovery, with  $f_i$  being the portion of the total protein population undergoing turnover process  $i$  ( $\sum_i f_i = 1$ ) and  $\tau_{d,i}$  being the characteristic dissociation time of process  $i$ . The characteristic dissociation time  $\tau_{d,i}$  is inverse to the turnover rate  $\omega_{d,i}$  and linked to the half-time reported in most FRAP experiments:  $\tau_{1/2} = \ln(2) \tau_d$ . If several molecular processes occur at similar time-scales, they cannot be distinguished, and the apparent rate constant measured reflects an average over all of the molecular processes acting at that time-scale. In practice, fluorescence recovery curves  $I(t)$  were fitted with an increasing number of exponential functions until the following three conditions were met: the goodness of fit estimated through  $r^2$  no longer increased, the total change in fluorescence associated with process  $i$  was less than 0.001%, and the sum of squared errors no longer decreased. Hence, this approach allowed determination of the number of molecular processes  $i$  that contribute to fluorescence recovery, their characteristic turnover times  $\tau_{d,i}$ , and the portion  $f_i$  of the total protein population that recovered through process  $i$ . In this analysis, changes in the recovery half-time  $\tau_{1/2}$  may have therefore resulted from changes in the number of processes  $i$  participating to recovery, changes in the characteristic times  $\tau_{d,i}$  of some or all of the processes, changes in the relative importance  $f_i$  of some or all of the turnover processes, or a combination of all of these factors. Logarithmic acceleration plots that represent the logarithm of the second derivative of the fit function were used to compare the turnover rate constants across experimental conditions and to visualize the different possible processes participating in the fluorescence recovery of the FRAP data. In these plots, each piecewise linear segment corresponds to a different fluorescence recovery process. The slope of each segment is characteristic for the turnover rate  $\omega_{d,i}$ . Notably, we only found formin-mediated actin kinetics in the stress fibers while two main processes corresponding to Arp2/3- and formin-filaments dominate the actin cortex.<sup>[22–24]</sup> Furthermore, cells showing significant spatial motion during an experiment were excluded from the analysis to avoid possible artefacts in the results.

**Quantification of F-actin Lengths:** Computation of the F-actin length distributions and their respective mean filament lengths were calculated from the actin turnover rates measured in the FRAP experiments as described in refs. [23,53].

**Photobleaching Optimization in Polyacrylamide Gel:** FRAP photobleaching volume calibration was performed using a 3D hydrogel substrate loaded with recombinant EGFP. Polyacrylamide (PAA) hydrogels were prepared as previously described.<sup>[55]</sup> Acrylamide (Sigma Aldrich) and bis-acrylamide (Sigma Aldrich) were combined at concentrations of 10% (vol/vol) and 0.4% (vol/vol) respectively, including the addition of  $1 \times 10^{-6}$  M EGFP (Sino Biological, China, Cat: 16118-S07E). Polymerization was initiated by the addition of TEMED (Sigma Aldrich) followed by APS (Sigma Aldrich). 3  $\mu$ L of the gel solution was pipetted onto an 18 mm coverslip and the drop covered by a 12 mm coverslip to form a sandwich. After allowing 30 min for polymerization, the gel was imaged at the microscope. Photobleaching calibration was performed using the AFM–FRAP platform where a circular ROI was created at varying laser powers for 2 s and the resulting bleach volume

imaged. Downstream analysis and visualization were performed using custom-written MATLAB (Mathworks) scripts.

**Statistical Analyses:** For each experimental condition, AFM-FRAP experiments were acquired from at least 12 individual cells over the course of at least three independent experiments. Statistical comparison of all conditions was carried out using a Kruskal-Wallis ANOVA test to detect a significant trend at the  $p < 0.01$  level (\*\*). Additionally, to test pair-wise significance Mann-Whitney U tests were performed and results were denoted as described in the legend of Figure 2 and Table 1. All statistical tests were applied using OriginPro 8.5.

## Acknowledgements

The authors thank the Wolfson Imaging Centre Oxford for providing microscope facility support, the Wellcome Trust (212343/Z/18/Z), and EPSRC (EP/S004459/1). The authors are also grateful for generous financial support from Andreas Janshoff from the Institute of Physical Chemistry at the University of Göttingen, Germany, and the DFG SFB 937. In addition, this work was supported by funding from the Engineering and Physical Sciences Research Council (EPSRC) and Medical Research Council (MRC) [grant number EP/L016052/1]. The authors also thank Richard Thorogate, Guillaume Charras, and Emad Moeendarbary from the London Centre for Nanotechnology and Mechanical Engineering Department at the University College London, UK, for equipment training and advice with the AFM analysis. M.F. designed and supervised the research. M.S. planned and executed the experiments and analyses. H.C.-Y. and L.B. helped with experiments. M.F. and M.S. wrote the manuscript.

## Conflict of Interest

The authors declare no conflict of interest.

## Keywords

actin cytoskeleton, AFM, cell mechanics, FRAP, kinetics, mechanobiology, turnover

Received: May 1, 2019

Revised: July 22, 2019

Published online: August 16, 2019

- [1] K. Rottner, F. Kage, *Curr. Biol.* **2017**, 27, R1274.
- [2] T. Luo, K. Mohan, P. A. Iglesias, D. N. Robinson, *Nat. Mater.* **2013**, 12, 1064.
- [3] H. Colin-York, Y. Javanmardi, M. Skamrahl, S. Kumari, V. T. Chang, S. Khuon, A. Taylor, T.-L. Chew, E. Betzig, E. Moeendarbary, V. Cerundolo, C. Eggeling, M. Fritzsche, *Cell Rep.* **2019**, 26, 3369.
- [4] A. R. Harris, P. Jreij, D. A. Fletcher, *Annu. Rev. Biophys.* **2018**, 47, 617.
- [5] I. V. Ogneva, *Biomed. Res. Int.* **2013**, 2013, 1.
- [6] M. Gupta, B. R. Sarangi, J. Deschamps, Y. Nematbakhsh, A. Callan-Jones, F. Margadant, R.-M. Mège, C. T. Lim, R. Voituriez, B.-T. Ladoux, *Nat. Commun.* **2015**, 6, 7525.
- [7] K. Hayakawa, H. Tatsumi, M. Sokabe, *Commun. Integr. Biol.* **2012**, 5, 572.
- [8] S. Tojkander, G. Gateva, A. Husain, R. Krishnan, P. Lappalainen, *eLife* **2015**, 4, e06126.
- [9] R. Oria, T. Wiegand, J. Escribano, A. Eloegui-Artola, J. J. Uriarte, C. Moreno-Pulido, I. Platzman, P. Delcanale, L. Albertazzi, D. Navajas, X. Trepas, J. M. García-Aznar, E. A. Cavalcanti-Adam, P. Roca-Cusachs, *Nature* **2017**, 552, 219.
- [10] C. S. Chen, *Nat. Rev. Mol. Cell Biol.* **2017**, 18, 715.
- [11] U. S. Schwarz, M. L. Gardel, *J. Cell Sci.* **2012**, 125, 3051.
- [12] D. Axelrod, D. E. Koppel, J. Schlessinger, E. Elson, W.W. Webb, *Biophys. J.* **1976**, 16, 1055.
- [13] M. Fritzsche, G. Charras, *Nat. Protoc.* **2015**, 10, 660.
- [14] F. Schneider, D. Waithe, B. C. Lagerholm, D. Shrestha, E. Sezgin, C. Eggeling, M. Fritzsche, *ACS Nano* **2018**, 12, 8540.
- [15] D. Blumenthal, L. Goldstien, M. Edidin, L. A. Gheber, *Sci. Rep.* **2015**, 5, 11655.
- [16] K. C. Mudumbi, E. C. Schirmer, W. Yang, *Nat. Commun.* **2016**, 7, 12562.
- [17] B. L. Sprague, R. L. Pego, D. A. Stavreva, J. G. McNally, *Biophys. J.* **2004**, 86, 3473.
- [18] E. A. J. Reits, J. J. Neefjes, *Nat. Cell Biol.* **2001**, 3, E145.
- [19] A. Bläzle, G. Soh, T. Braun, D. Mörsdorf, H. Preiß, B. M. Jordan, P. Müller, *Nat. Commun.* **2018**, 9, 1582.
- [20] P. Muller, K. W. Rogers, B. M. Jordan, J. S. Lee, D. Robson, S. Ramanathan, A. F. Schier, *Science* **2012**, 336, 721.
- [21] M. Kang, C. A. Day, A. K. Kenworthy, E. DiBenedetto, *Traffic* **2012**, 13, 1589.
- [22] M. Fritzsche, A. Lewalle, T. Duke, K. Kruse, G. Charras, *Mol. Biol. Cell* **2013**, 24, 757.
- [23] M. Fritzsche, C. Erlenkämper, E. Moeendarbary, G. Charras, K. Kruse, *Sci. Adv.* **2016**, 2, e1501337.
- [24] M. Fritzsche, D. Li, H. Colin-York, V. T. Chang, E. Moeendarbary, J. H. Felce, E. Sezgin, G. Charras, E. Betzig, C. Eggeling, *Nat. Commun.* **2017**, 8, 14347.
- [25] M. B. Smith, T. Kiuchi, N. Watanabe, D. Vavylonis, *Biophys. J.* **2013**, 104, 247.
- [26] G. Dimchev, A. Steffen, F. Kage, V. Dimchev, J. Pernier, M.-F. Carlier, K. Rottner, *Mol. Biol. Cell* **2017**, 28, 1311.
- [27] E. Moeendarbary, A. R. Harris, *WIREs Syst. Biol. Med.* **2014**, 6, 371.
- [28] S. Sen, S. Subramanian, D. E. Discher, *Biophys. J.* **2005**, 89, 3203.
- [29] F. Eghiaian, F. Rico, A. Colom, I. Casuso, S. Scheuring, *FEBS Lett.* **2014**, 588, 3631.
- [30] A. J. Katan, C. Dekker, *Cell* **2011**, 147, 979.
- [31] T. Ando, *Biophys. Rev.* **2017**, 9, 421.
- [32] G. T. Charras, M. A. Horton, *Biophys. J.* **2002**, 82, 2970.
- [33] K. Mollaeian, Yi Liu, S. Bi, Y. Wang, J. Ren, M. Lu, *Int. J. Mater. Sci.* **2018**, 19, 3461.
- [34] J. B. Wyckoff, Y. Wang, E. Y. Lin, J.-F. Li, S. Goswami, E. R. Stanley, J. E. Segall, J. W. Pollard, J. Condeelis, *Cancer Res.* **2007**, 67, 2649.
- [35] D. V. Köster, K. Husain, E. Iljazi, A. Bhat, P. Bieling, R. D. Mullins, M. Rao, S. Mayor, *Proc. Natl. Acad. Sci. USA* **2016**, 113, E1645.
- [36] L. Blanchoin, R. Boujemaa-Paterski, C. Sykes, J. Plastino, *Physiol. Rev.* **2014**, 94, 235.
- [37] D. A. Fletcher, R. D. Mullins, *Nature* **2010**, 463, 485.
- [38] P. Chugh, A. G. Clark, M. B. Smith, D. A. D. Cassani, K. Dierkes, A. Ragab, P. P. Roux, G. Charras, G. Salbreux, E. K. Paluch, *Nat. Cell Biol.* **2017**, 19, 689.
- [39] M. R. Stachowiak, M. A. Smith, E. Blankman, L. M. Chapin, H. E. Balcioglu, S. Wang, M. C. Beckerle, B. O'Shaughnessy, *Proc. Natl. Acad. Sci. USA* **2014**, 111, 17528.
- [40] E. M. De La Cruz, M. L. Gardel, *J. Biol. Chem.* **2015**, 290, 17137.
- [41] E. L. Elson, G. M. Genin, *Exp. Cell Res.* **2013**, 319, 2490.
- [42] J. Stricker, T. Falzone, M. L. Gardel, *J. Biomech.* **2010**, 43, 9.
- [43] K. Burridge, E. S. Wittchen, *J. Cell Biol.* **2013**, 200, 9.
- [44] S. Walcott, S. X. Sun, *Proc. Natl. Acad. Sci. USA* **2010**, 107, 7757.
- [45] W. M. McFadden, P. M. McCall, M. L. Gardel, E. M. Munro, *PLoS Comput. Biol.* **2017**, 13, e1005811.
- [46] M. Fritzsche, R. A. Fernandes, V. T. Chang, H. Colin-York, M. P. Clausen, J. H. Felce, S. Galiani, C. Erlenkämper, A. M. Santos, J. M. Heddleston, I. Pedroza-Pacheco, D. Waithe, J. B. de la Serna, B. C. Lagerholm, T.-L. Liu, T.-L. Chew, E. Betzig, S. J. Davis, C. Eggeling, *Sci. Adv.* **2017**, 3, e1603032.



- [47] M. P. Clausen, H. Colin-York, F. Schneider, C. Eggeling, M. Fritzsche, *J. Phys. D: Appl. Phys.* **2017**, 50, 064002.
- [48] G. H. Koenderink, E. K. Paluch, *Curr. Opin. Cell Biol.* **2018**, 50, 79.
- [49] S. P. Romero, C. Le Clainche, D. Didry, C. Egile, D. Pantaloni, M.-F. Carlier, *Cell* **2004**, 119, 419.
- [50] H. Kubota, M. Miyazaki, T. Ogawa, T. Shimozawa, K. Kinoshita, S. I. Ishiwata, *Biophys. J.* **2017**, 113, 461.
- [51] C. Higashida, T. Kiuchi, Y. Akiba, H. Mizuno, M. Maruoka, S. Narumiya, K. Mizuno, N. Watanabe, *Nat. Cell Biol.* **2013**, 15, 395.
- [52] A. Jégou, M.-F. Carlier, G. Romet-Lemonne, *Nat. Commun.* **2013**, 4, 1883.
- [53] B. R. Brückner, H. Nöding, M. Skamrahl, A. Janshoff, *Prog. Biophys. Mol. Biol.* **2019**, 144, 77.
- [54] M. Fritzsche, R. A. Fernandes, V. T. Chang, H. Colin-York, M. P. Clausen, J. H. Felce, S. Galiani, C. Erlenkämper, A. M. Santos, J. M. Heddleston, I. Pedroza-Pacheco, D. Waithe, J. B. de la Serna, B. C. Lagerholm, T.-L. Liu, T.-L. Chew, E. Betzig, S. J. Davis, C. Eggeling, *Sci. Adv.* **2017**, 3, e1603032.
- [55] H. Colin-York, C. Eggeling, M. Fritzsche, *Nat. Protoc.* **2017**, 12, 783.